Mechanics of Materials 80 (2015) 255–263

Contents lists available at ScienceDirect

Mechanics of Materials

journal homepage: www.elsevier.com/locate/mechmat

A model coupling plasticity and phase transformation with application to dynamic shear deformation of iron

Amir Sadjadpour [a], Daniel Rittel [b], Guruswami Ravichandran [c,*], Kaushik Bhattacharya [c]

[a] TMT Observatory Corporation, Pasadena, CA 91105, United States
[b] Technion – Israel Institute of Technology, Technion City, Haifa 32000, Israel
[c] California Institute of Technology, 2100 E California Blvd, Pasadena, CA 91125, United States

ARTICLE INFO

Article history:
Received 31 October 2013
Received in revised form 8 April 2014
Available online 4 May 2014

We dedicate this paper to Alain Molinari on the occasion of his 65th birthday for his contributions to many areas of mechanics of materials, particularly to dynamic deformation and adiabatic shear localization.

Keywords:
Plasticity
Phase transformation
Dynamic deformation
Iron

ABSTRACT

A simple model that brings together well-established thermo-mechanical models of plasticity with those of martensitic phase transformation into a single thermodynamic framework is proposed. The presentation is in one space dimension, but the framework is general so that the model may be extended to higher dimensions. The model is used to study recent experiments on the $\alpha \Longleftrightarrow \epsilon$ martensitic phase transformation of pure iron under dynamic, shear-dominant loading conditions. It is shown that the model fitted to established thermodynamic data and selected experiments is able to reproduce the experimental observations in a wide range of loading rates ranging from quasistatic to $10^4\ s^{-1}$ as well as a wide range of phenomena ranging including overall rate hardening and thermal softening. In doing so, the model also provides new insight into the $\alpha \Longleftrightarrow \epsilon$ phase transformation in iron.

1. Introduction

The mechanical properties of pure iron have been extensively studied in the past decades mostly in the context of its response at high strain-rates and pressures (see for example Follansbee, 1989; Jia et al., 2000; Klepaczcko, 1969; Mason and Worswick, 2001; Nicolazo and Leroy, 2002; Ostwaldt et al., 1997; Watson, 1970; Weston, 1992). The high pressure is applied either in a quasi-static way using a diamond anvil press, or using shock wave for example in plate-impact experiments of a very short duration (Clifton and Klopp, 1985; Murr and Esquivel, 2004; Rosenberg et al., 1980). Since the shock wave techniques are more accessible than the quasi-static experiments, a major part of the literature reports results obtained using shock experiments (Bancroft et al., 1956; Kalantar et al., 2005; Millett et al., 1997; Ostwaldt et al., 1997; Sano et al., 2003; Yaakobi et al., 2005).

One of the main points of interest is the existence of an allotropic α (BCC) $\Longleftrightarrow$ ε (HCP) phase transition in this material (Ahrens et al., 2002). This phase transformation, discovered by Bancroft et al. (1956), is known to be reversible, and occurs at large pressures, starting at 13 GPa and completing around 23 GPa in high pressure compression experiments. While much of the literature considered hydrostatic pressure as the trigger for the phase transformation, Jones and Graham (1968) pointed out the role of shear that is inherent in high pressure experiments (see also direct measurements by Millett et al. (1997)). So, recent work has focused on the role of shear stresses in determining the critical pressure for the onset of the phase

* Corresponding author.
E-mail address: ravi@caltech.edu (G. Ravichandran).

http://dx.doi.org/10.1016/j.mechmat.2014.04.010
0167-6636/

transformation. Specifically, Von Barge and Boehler (1990) have shown that shear stresses in the pressure transmitting medium systematically affect the transformation pressure and hysteresis loop observed upon unloading. Further, atomistic calculations have shown the significant contribution of the shear strain, even of modest magnitude, to the $\alpha \iff \varepsilon$ transition (Caspersen et al., 2004; Lew et al., 2006). Still, the experimental literature on direct observations of the phase transition, or on the role of shear on its occurrence, is still scarce (Kalantar et al., 2005; Sano et al., 2003). For example, real-time diffraction experiments like those of Kalantar et al. (2005), who confirmed the existence of the phase transition, do not address the role of shear in the phase transformation process.

Rittel et al. (2006) conducted a comprehensive series of dynamic shear experiments on pure iron using the shear-compression specimen (SCS) in a split Hopkinson (Kolsky) pressure bar. Due to the reversibility of the phenomenon, those authors could not provide a direct evidence of phase transformation, but several indirect observations supported the likelihood of the claim. Specifically, it was observed that at very high strain rates (of the order of 8000 s^{-1}), pure iron would exhibit a negative strain-hardening response from the onset of yielding. Further, the measured value Taylor–Quinney factor (Taylor and Quinney, 1934) (which describes the amount of plastic work that is converted to heat) would exceed unity thereby suggesting that some latent heat was injected into the system.

In this paper, we develop a simple model that combines martensitic phase transformations with plasticity, and uses it to study the experiments of Rittel et al. (2006). The model builds on the formulation of rate-dependent thermoplasticity proposed by Rosakis et al. (2000) and that of martensitic phase transformations by Sadjadpour and Bhattacharya (2007). We introduce internal variables to describe the phase transformation and plasticity, place them on a consistent thermodynamic setting and prescribe appropriate evolution laws – stick slip style for the phase transformation and Johnson–Cook for the plasticity. We then specialize the model to a homogenous, adiabatic, constant strain rate setting as is appropriate for the experimental setting. We fit the model to well-known thermodynamic properties of iron, as well as selected experimental observations, and show that the model is capable of capturing the entire range of experimental observations. While the development of such a model is not conclusive in establishing that allotropic phase transition actually occurs in iron as a result of shear loading, it nevertheless adds to the growing evidence establishing its feasibility.

Various authors have studied the coupling between plasticity and martensitic phase transformation. Much of this work is motivated by transformation induced plasticity (TRIP) in steels where a non-transforming ferritic matrix contains transforming inclusions and the transformation in the transforming grains leads to plastic deformation in both the grains and the surrounding matrix (e.g. Fischer et al., 2000; Cherkaoui et al., 2000; Turteltaub and Suiker, 2005; Leblond et al., 1989; Leblond, 1989; Levitas et al., 1998). This work seeks to understand the nature of the plastic deformation, as well its effect on overall properties. There is also an emerging literature how martensitic laths contribute ductile fracture (Shanthraj and Zikry, 2013), and the interplay of plasticity and phase transformations in shape-memory alloys (Richards et al., 2013). These do not address the α–ϵ transformation in iron. Barton et al. (2005) developed a continuum model (in a crystal plasticity type setting) for this transformation and used it to study shock-induced transformation and texture evolution. Similarly, Caspersen et al. (Caspersen et al., 2004; Lew et al., 2006) developed a multiscale model for this phenomena. However these models are quite involved. In contrast, the model we present is limited in scope, but simple. Yet, it retains enough physics to enable us to analyze the shear-dominant experiments described above and to provide insights into the transformation and the thermomechanical coupling.

The paper is organized as follows. Section 2 introduces the model and describes its thermodynamic setting. In Section 3 we fit the model to experimental observations and then study the response of the material under a number of strains-controlled tests. We conclude in Section 4 with a brief discussion.

2. A thermo-mechanical model

In this section we develop and discuss our phenomenological constitutive model within a continuum thermodynamic framework. The model builds on the formulation of rate-dependent thermoplasticity proposed by Rosakis et al. (2000) and martensitic phase transformations by Sadjadpour and Bhattacharya (2007).

2.1. Kinematics

We work in the one dimensional setting. We denote by $u(x,t)$ the displacement at particle x at time t and by $\varepsilon(x,t)$ the strain. We assume that the strain can be additively decomposed into elastic, transformation and plastic strains:

$$\varepsilon(x,t) = \varepsilon_e(x,t) + \lambda(x,t)\varepsilon_m(x,t) + \varepsilon_p(x,t), \tag{1}$$

where ε_e is the elastic strain, λ is the volume fraction of martensite, ε_m is the transformation strain associated with the martensite and ε_p is the plastic strain. Note that we are in the coarse-grained setting on a length scale of multiple grains so that we do not resolve the details of the martensitic microstructure and grains. Thus, $\lambda(x,t)$ is the volume fraction averaged over a representative volume element (RVE) associated with the particle x at time t while ε_m is the average transformation strain of every subregion of martensite in the RVE. Consequently, they satisfy the constraints

$$\lambda \in [0,1] \quad \text{and} \quad \varepsilon_m \in [\varepsilon_m^-, \varepsilon_m^+], \tag{2}$$

where the parameter $\varepsilon_m^- < 0 < \varepsilon^+ 0$ depends on the crystallography and texture of the material. Further, the total transformation strain of the RVE is $\lambda\varepsilon_m$ (Sadjadpour and Bhattacharya, 2007).

We also introduce an internal variable $\zeta(x,t)$ that describes the state of plastic work hardening at point x at time t.

2.2. Balance laws

We assume that the usual balance laws hold. In local form, the balance of linear momentum and energy may be stated as

$$\rho\ddot{u} = \sigma_{,x}, \tag{3}$$

$$\dot{e} = -q_{,x} + r + \sigma\dot{\varepsilon}, \tag{4}$$

where ρ is the (referential) mass per unit length, σ is the (Piola–Kirchhoff) stress, e denotes the internal energy density, q the heat flux and r the radiative heating. Also, superposed dots denote differentiation with respect to time while the subscript comma denotes differentiation with respect to the variables that follow. We also use the local form of the second law of thermodynamics (Clausius–Duhem inequality),

$$-\dot{W} - \eta\dot{\theta} + \sigma\dot{\varepsilon} - \frac{q\theta_{,x}}{\theta} \geqslant 0, \tag{5}$$

where $W = e - \theta\eta$ is the Helmholtz free energy density, η the entropy density and θ the (absolute) temperature.

2.3. Constitutive relations

We assume that the Helmholtz free energy density depends on the strain, the temperature and the internal variables (λ, ε_m, ε_p and ζ):

$$W = W(\varepsilon, \lambda, \varepsilon_m, \varepsilon_p, \zeta, \theta). \tag{6}$$

Specifically, we assume

$$W = \frac{E}{2}(\varepsilon - \varepsilon_p - \lambda\varepsilon_m)^2 + \lambda\omega(\theta) - c_p\theta\ln\left(\frac{\theta}{\theta_0}\right) + W_p(\zeta), \tag{7}$$

where E is the elastic modulus, ω is the difference in chemical energy between the austenite and the martensite, c_p is the heat capacity and θ_0 is the reference (absolute) temperature.

The first term is the elastic energy. In this work, we have assumed for simplicity that the elastic modulus is equal in both the austenite and the martensite, and that it remains unchanged with stress. This is justified for the small stresses that we encounter in this work, and should be replaced with a phase-aware equation of state if higher stresses are present. The second term is the chemical energy of phase transformation defined as the excess free energy due to the transformation from austenite to martensite. Therefore, this term is proportional to the volume fraction λ. Further, this contribution is primarily entropic and is related to the latent heat. Therefore, we further assume that

$$\omega(\theta) = \frac{L}{\theta_{cr}}(\theta - \theta_{cr}), \tag{8}$$

where L is the latent heat of transformation and θ_{cr} is the thermodynamic transformation temperature. The third term is the contribution due to specific heat, and this is again taken to be equal in both the martensite and austenite for simplicity. The final term W_p is the stored energy of plastic work. We will assume a specific form in the sequel.

Notice that we have neglected ordinary thermal expansion, the temperature dependance of the stored energy of plastic work and the direct energetic interaction between martensitic phase transitions and plasticity. We comment on these later.

We substitute the Helmholtz free energy density relation (7) in the second law and use arguments similar to those of Coleman and Noll (1963) to obtain

$$\sigma = \frac{\partial W}{\partial\varepsilon} = E(\varepsilon - \varepsilon_p - \lambda\varepsilon_m), \tag{9}$$

$$\eta = -\frac{\partial W}{\partial\theta} = -\lambda\frac{L}{\theta_{cr}} + c_p\left(1 + \ln\left(\frac{\theta}{\theta_0}\right)\right). \tag{10}$$

We assume that the heat flux is given by Fourier Law:

$$q = -K\theta_{,x}, \tag{11}$$

where K is thermal conductivity (assumed to be equal in both the austenite and the martensite).

It remains to specify evolution laws for the internal variables. To do so, we identify the driving forces

$$d_m := -\frac{\partial W}{\partial\varepsilon_m} = \lambda\sigma, \tag{12}$$

$$d_\lambda := -\frac{\partial W}{\partial\lambda} = \sigma\varepsilon_m - \omega, \tag{13}$$

$$d_p := -\frac{\partial W}{\partial\varepsilon_p} = \sigma, \tag{14}$$

$$d_\zeta := -\frac{\partial W}{\partial\zeta} = -\frac{\partial W_p}{\partial\zeta} \tag{15}$$

and postulate kinetic relations

$$\dot{\varepsilon}_m := f_m(d_m, \varepsilon, \lambda, \varepsilon_m, \varepsilon_p, \zeta, \theta), \tag{17}$$

$$\dot{\lambda} = f_\lambda(d_\lambda; \varepsilon, \lambda, \varepsilon_m, \varepsilon_p, \zeta, \theta), \tag{18}$$

$$\dot{\varepsilon}_p := f_p(d_p, \varepsilon, \lambda, \varepsilon_m, \varepsilon_p, \zeta, \theta), \tag{19}$$

$$\dot{\zeta} := f_\zeta(d_\zeta, \varepsilon, \lambda, \varepsilon_m, \varepsilon_p, \zeta, \theta). \tag{20}$$

Note that we have assumed for now that the kinetic relations can depend explicitly on the state of the system. The second law requires that the kinetic relations satisfy

$$f_m d_m + f_\lambda d_\lambda + f_p d_p + f_\zeta d_\zeta \geqslant 0 \tag{21}$$

and this places restrictions on the kinetic relations.

2.3.1. Phase transformation

We assume that the martensite reorients itself very fast so that the evolution of ε_m is instantaneous. Therefore, we assume following (Sadjadpour and Bhattacharya, 2007) that

$$\varepsilon_m = \begin{cases} \varepsilon_m^- & \sigma < 0, \\ \varepsilon_m^+ & \sigma > 0. \end{cases} \tag{22}$$

Further, we assume that the kinetic relation f_λ describing the evolution of the martensite volume fraction λ is taken to be the following:

$$\dot{\lambda} = \begin{cases} \dot{\lambda}^+ \left(1 + \left(d_\lambda - d_\lambda^+\right)^{-1}\right)^{-\frac{1}{p}} & d_\lambda > d_\lambda^+ \text{ and } \lambda < 1, \\ \dot{\lambda}^- \left(1 + \left(d_\lambda^- - d_\lambda\right)^{-1}\right)^{-\frac{1}{p}} & d_\lambda < d_\lambda^- \text{ and } \lambda > 0, \\ 0 & \text{otherwise.} \end{cases} \tag{23}$$

where $\dot{\lambda}^\pm$, $d_\lambda^\pm$, p are material parameters. This relation is shown in Fig. 1. Note that this law is rate-independent with critical force for small rates, but becomes rate dependent at high rates. In brief, the rate-independence with critical force reflects a combination of metastability and pinning by defects. The rate-dependent nature of the law at large driving forces is based on the observations that suggest the phase boundaries require an unboundedly increasing driving force for the propagation speeds to reach towards some sound speed.

2.3.2. Plasticity

We now turn to f_p and f_ζ and follow Rosakis et al. (2000). In light of (9) and the fact that $W_p = W_p(\zeta, \theta)$, we can write

$$f_p = f_p(\sigma, \zeta, \theta), \quad f_\zeta = f_\zeta(\sigma, \zeta, \theta). \tag{24}$$

We assume that

$$f_p(\sigma, \zeta, \theta) = \operatorname{sign}(\sigma) f_\zeta(\sigma, \zeta, \theta). \tag{25}$$

Note that this is equivalent to $\dot{\zeta} = |\dot{\varepsilon}_p|$ or identifying the plastic hardening variable with the accumulated plastic strain (Rosakis et al., 2000). We now assume that the function f_ζ may be specified in terms of a yield stress $\tau(\zeta, \theta) > 0$ and non-decreasing hardening function H that satisfies $H(x) = 0$ for all $x \leqslant 0$:

$$f_\zeta = H\left(\frac{|\sigma|}{\tau(\zeta, \theta)} - 1\right). \tag{26}$$

We further assume strain hardening and thermal softening:

$$\tau_{,\zeta} \geqslant 0, \quad \tau_{,\theta} \leqslant 0. \tag{27}$$

We further assume that the hardening function H satisfies

$$H'(x) > 0 \quad \forall x \geqslant 0. \tag{28}$$

When $|\sigma| \geqslant \tau$, we can invert (26) to write after using (20)

$$|\sigma| = \tau(\zeta, \theta)\left(H^{-1}(\dot{\zeta}) + 1\right). \tag{29}$$

For the specific forms of ζ and H, we adapt the widely used Johnson and Cook (1985) flow rule as modified by Vural et al. (2003) to include both the quasistatic and dynamics regimes:

$$|\sigma| = (\sigma_0 + B\zeta^n)\left(1 + C \ln\left(\frac{\dot{\zeta}_p}{\dot{\zeta}_0}\right)\right)\left(\frac{1 - D\exp(\theta_*)^m}{1 - D}\right), \tag{30}$$

where

$$\theta_* = \left(\frac{\theta - \theta_r}{\theta_r - \theta_m}\right), \tag{31}$$

$$C = C^q + \frac{C^d - C^q}{2}\left(1 + \tanh\left(\ln\frac{\dot{\zeta}}{\dot{\zeta}_\star}\right)\right), \tag{32}$$

$$\dot{\zeta}_0 = \dot{\zeta}_0^q + \frac{\dot{\zeta}_0^d - \dot{\zeta}_0^q}{2}\left(1 + \tanh\left(\ln\frac{\dot{\zeta}}{\dot{\zeta}_\star}\right)\right) \tag{33}$$

and σ_0, B, n, C^q, C^d, $\dot{\zeta}_0^q$, $\dot{\zeta}_0^d$, $\dot{\zeta}_\star$, D, m, θ_r and θ_m are material parameters. θ_r is the reference temperature at which σ_0 is measured and θ_m is the melting temperature of the material; further notice that the relations (32) and (33) smoothly transitions from the quasistatic values C^q, $\dot{\zeta}_0^q$ and the dynamic values C^d, $\dot{\zeta}_0^d$ at the critical strain rate $\dot{\zeta}_\star$.

Finally, we turn to the stored energy of plastic work W_p. Note that the rate of plastic working is $\sigma\dot{\varepsilon}_p$, some of which is stored at a rate $\dot{W}_p$ while the rest is converted to heat. Therefore, we define *the Taylor–Quinney factor* or the instantaneous or differential fraction of plastic work[1] that is converted to heat (Taylor and Quinney, 1934; Farren and Taylor, 1925) to be

$$\beta = 1 - \frac{\dot{W}_p}{\sigma\dot{\varepsilon}_p}. \tag{34}$$

Since the Clausius–Duhem inequality (5) must hold for all, processes including adiabatic processes ($q = 0$) with no phase transition ($\dot{\lambda} = 0$), it follows that $\sigma\dot{\varepsilon}_p - \dot{W}_p \geqslant 0$ so that $0 \leqslant \beta \leqslant 1$.

Recalling (7), (25) and (30), and also assuming that the stress is larger than the yield stress, we assume

$$\beta = 1 - \frac{\frac{\partial W_p}{\partial \zeta}\dot{\zeta}}{|\sigma|\dot{\zeta}} = 1 - \frac{\frac{\partial W_p}{\partial \zeta}(\zeta)}{|\sigma|(\zeta, \dot{\zeta}, \theta)} = \beta(\zeta, \dot{\zeta}, \theta). \tag{35}$$

We specify W_p using β, but only for a particular setting described below.

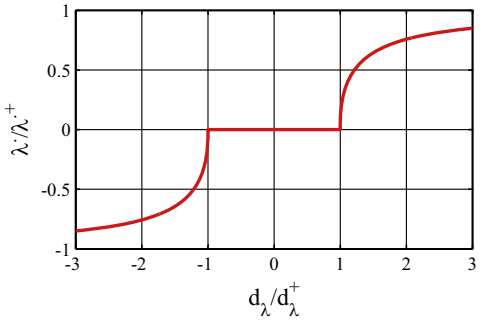

Fig. 1. The kinetic relation between $\dot{\lambda}$ and the driving force d_λ.

2.4. Homogenous, adiabatic, constant strain-rate process

We seek to apply this model to experiments conducted with shear-compression specimens in a split Hopkinson

[1] We note that our definition differs from one used in experimental works as the ratio of the rate of change of thermal energy to the rate of plastic working. These are equivalent in the absence of phase transformations, but differ in the presence of phase transformations as we describe in detail in Section 2.5.

(Kolsky) bar. This experiment probes the material in the gage section in a homogeneous, adiabatic, constant strain-rate process. So we specialize our model to this setting. Since the process is homogeneous and adiabatic, $q = r = 0$. Further, since the strain-rate is constant, the strain is monotone increasing. We make the stronger assumption that the plastic strain is also monotone so that we identify the plastic strain with the accumulated plastic strain,

$$\zeta = \varepsilon_p, \quad \dot{\zeta} = \dot{\varepsilon}_p. \tag{36}$$

For a homogenous, adiabatic and constant strain-rate process, Rosakis et al. (2000) showed that one can express the fraction of plastic work converted to heat as simply a function of strain and strain-rate: $\beta = \beta(\varepsilon_p, \dot{\varepsilon_p})$. Therefore, we make the final constitutive assumption motivated by their experiments:

$$\beta = \beta_0 \left(\frac{\dot{\varepsilon}_p}{\dot{\varepsilon}_p^{+}}\right)^2 \left(1 + \beta_1 \varepsilon_p (\varepsilon_p^{\star} - \varepsilon_p)\right), \tag{37}$$

where β_0, β_1, ε_p^{+} and $\varepsilon_p^{\star}$ are parameters. Note that β increases with increasing strain-rate, and initially increases but subsequently decreases with strain.

With β defined, we now turn to solving the governing equation. With the assumption of constant strain-rate, the balance of momentum (3), is automatically satisfied. So, it only remains to examine the energy balance (4). Recalling that $q = r = 0$ and substituting for the internal energy in terms of the Helmholtz free energy and entropy, this equation becomes

$$\dot{W} + \theta\dot{\eta} + \dot{\theta}\eta = \sigma\dot{\varepsilon}. \tag{38}$$

Using the constitutive assumption (7) for W to expand $\dot{W}$ and recalling the definitions (9), (10) and the driving forces, we obtain

$$c_p\dot{\theta} = \dot{\lambda}\theta\frac{L}{\theta_{cr}} + d_m\dot{\varepsilon}_m + d_\lambda\dot{\lambda} + d_p\dot{\varepsilon}_p + d_\zeta\dot{\zeta}. \tag{39}$$

We recall the expressions for d_p, d_ζ in (14), (15) as well as the definition of β in (34), to rewrite sum of the final two terms as $\beta\sigma\varepsilon_p$. Finally, we neglect the kinetic dissipation of martensitic transformation, $d_m\dot{\varepsilon}_m + d_\lambda\dot{\lambda}$, which is typically small compared to the latent heat. We obtain,

$$c_p\dot{\theta} = \theta\dot{\lambda}\frac{L}{\theta_{cr}} + \beta\sigma\dot{\varepsilon}_p. \tag{40}$$

In summary, for a homogenous, adiabatic, constant strain-rate process with sufficiently high stresses so that plasticity is active, we solve (9), (23), (30), and (40).

2.5. Apparent Taylor–Quinney factor

We conclude this section with a comment on the Taylor–Quinney factor β defined in (34). We note here that this factor can *not* be measured directly in experiment by measuring the temperature and using the energy balance due to the presence of the latent heat during phase transformation. Following common experimental practice (e.g., Rosakis et al., 2000; Rittel et al., 2006), we define a new variable, the apparent Taylor–Quinney factor as

$$\beta_{\text{app}} = \frac{c_p\dot{\theta}}{\sigma\dot{\varepsilon}_p}. \tag{41}$$

Using (40), we see that

$$\beta_{\text{app}} = \beta + \frac{L\dot{\lambda}\theta}{\theta_{cr}\sigma\dot{\varepsilon}_p}. \tag{42}$$

Thus, in the presence of phase transformation, the apparent Taylor–Quinney factor differs from the theoretical one due to the addition of latent heat. Thus, even if $0 \leqslant \beta \leqslant 1$ as discussed earlier, β_{app} can exceed unity in the presence of a phase transformation. Therefore $\beta_{\text{app}} > 1$ can be interpreted as the presence of phase transition.

3. Illustration

In this section, we demonstrate that our model is consistent with the observed stress–strain and thermal response of pure iron for a wide range of strain rates. We fit the model to selected tests, and then hold the parameters fixed during the rest of the section. We find that the model is able to capture thermal softening, rate hardening, and observed trends in the apparent Taylor–Quinney factor.

3.1. Experiment

The experimental procedure is presented in detail in Rittel et al. (2006), and is only briefly outlined here. The quasistatic experimental results carried out on a servo-hydraulic MTS machine under displacement control, and high strain rate compressive testings are carried out using a split Hopkinson (Kolsky) pressure bar. A shear-compression specimen (Rittel et al., 2002) – a cylinder in which two diametrically opposed slots are machined at an angle with respect to the longitudinal axis to the test gage section – was used. This specimen enables testing up to large strains of $O(1)$ over a large range of strain rates in a state of dominant shear. However, the state of stress is not pure shear, and therefore the recorded load–displacement data is presented as (Mises) equivalent stress and strain. The surface temperature of the gauge section was measured in situ using a liquid nitrogen cooled mercuric cadmium telluride (MCT) infrared detector covering an area of 1 mm^2. The simultaneous determination of the equivalent stress–strain and temperature in the gauge section was later processed to determine the apparent Taylor–Quinney factor β_{app}.

3.2. Parameters

Consistent with typical experiments on pure iron (see for example Chen and Ahrens, 1996), we consider the following parameter values:

$$\rho = 7870\ \text{kg/m}^3, \quad E = 190\ \text{GPa},$$
$$c_p = 3.5\ \text{MJ/K/m}^3, \quad \text{and} \quad L = -1.07 \times 10^8\ \text{J/m}^3.$$

In all the simulations ambient temperature is assumed to be equal to 295 K. We further assume that ε_m is equal to zero for the α phase and equal to 0.5 for the ε phase. Critical temperature θ_{cr} is assumed to be equal to 800 °K. We also assume the following kinetic coefficients:

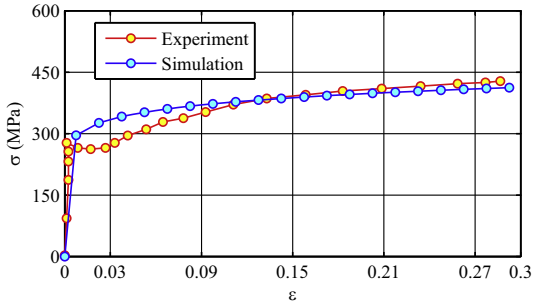

Fig. 2. Quasistatic stress–strain response of pure iron.

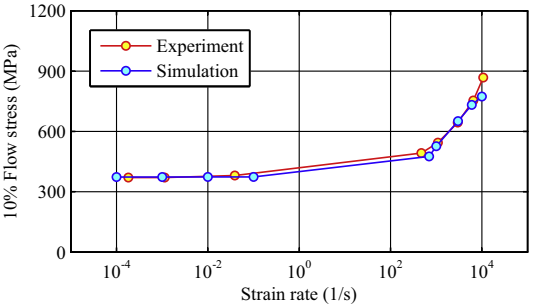

Fig. 3. Flow stress dependence on strain rate.

$$\dot{\lambda}^{+} = -\dot{\lambda}^{-} = 1\ \mathrm{s}^{-1}, \quad d_{\lambda}^{+} = -d_{\lambda}^{-} = 2.9 \times 10^{8}\ \mathrm{J/m}^{3}, \quad p = 2.$$

We now turn to fitting the Johnson–Cook flow model. The first three parameters, σ_0, B and n, are determined from quasistatic tests. Fig. 2 shows results of the experimental observations and the model fit to the following parameters:

$$\sigma_0 = 32.6\mathrm{MPa}, \quad B = 430\mathrm{MPa}, \quad n = 0.1.$$

We turn to a combination of quasistatic and dynamic tests (at moderate strain rates to fit the next set of coefficients C^q, C^d, $\dot{\zeta}_0^q$, $\dot{\zeta}_0^d$, $\dot{\zeta}_\star$ that determine the role of strain rate. Fig. 3 shows results of experimental observation and the model fit to the following parameters:

$$\dot{\zeta}_0^q = 4 \times 10^{-5}\ \mathrm{s}^{-1}, \quad \dot{\zeta}_0^d = 355\ \mathrm{s}^{-1}, \quad C^q = .00008,$$
$$C_2 = .385, \quad \dot{\zeta}_\star = 100\ \mathrm{s}^{-1}.$$

Finally, we fit the coefficients that determine the temperature dependance. Fig. 4 shows results of experimental observation and the model fit to the following parameters:

$$m = -9, \quad D = -4, \quad \theta_r = 295K, \quad \theta_m = 1811\ \mathrm{K}.$$

Finally, we fit the parameters for β defined in (37). We do so by trial and error to be

$$\beta_0 = 0.5, \quad \dot{\varepsilon}_p^{+} = 1\ \mathrm{s}^{-1}, \quad \beta_1 = 0.5, \quad \varepsilon_p^{\star} = 1. \tag{43}$$

Fig. 5 shows β as a function of strain ε for three different strain rates.

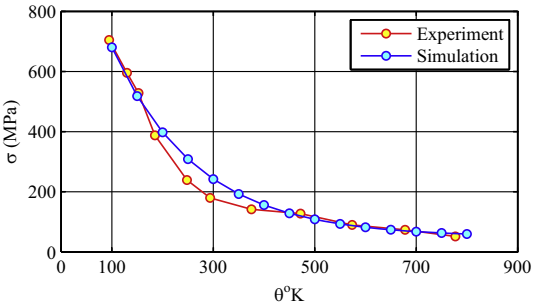

Fig. 4. Temperature dependence of the yield stress.

3.3. Strain-controlled tests

We now demonstrate the stress–strain response of pure iron for a wide range of strain rates. We are interested in strains of the order of tens of percents and specifically the behavior at yield and beyond. Therefore, we ignore the elastic strain. In other words, we assume that the imposed strain is a sum of transformation and plastic strains. For each simulation we compare our results with experimental observations of Rittel et al. (2006) (see Figs. 6–13).

Fig. 6 shows the quasi-static response, while Figs. 7–13 show the response at progressively increasing strain rate from 2800 to 10,000 s^{-1}. In each figure, we show both the results of the model and the experimental observations, and note good agreement between them. First, we

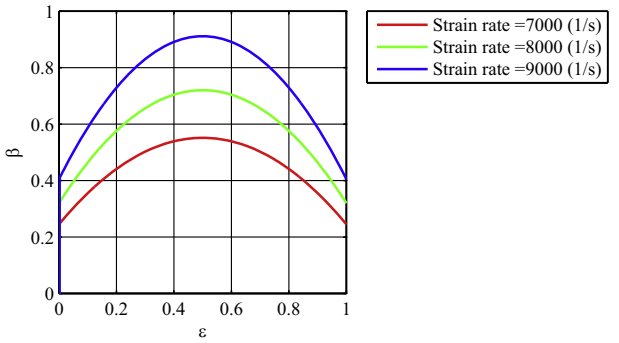

Fig. 5. Schematic contribution of plastic work in generating heat as a function of strain and strain rate.

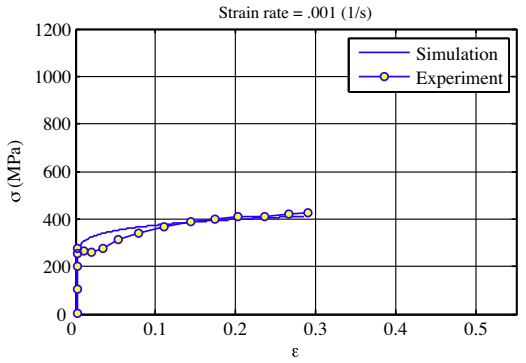

Fig. 6. Stress–strain response of pure iron for a quasistatic test.

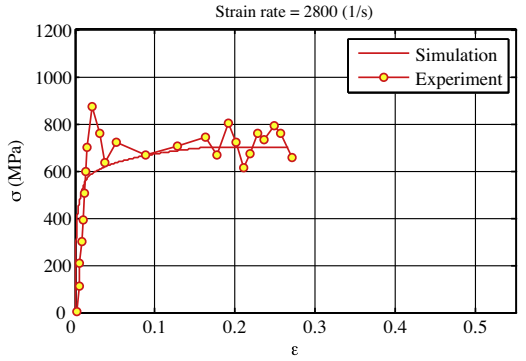

Fig. 7. Stress–strain response of pure iron for a dynamic test, $\dot{\varepsilon} = 2800(\frac{1}{s})$.

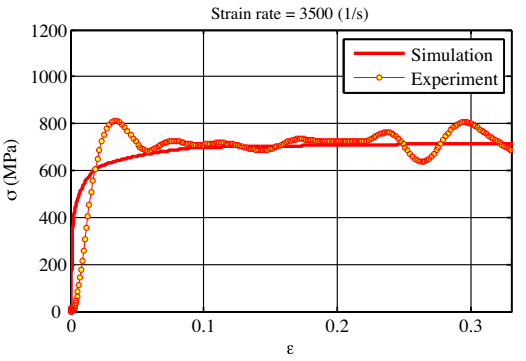

Fig. 8. Stress–strain response of pure iron for a dynamic test, $\dot{\varepsilon} = 3500(\frac{1}{s})$.

see that the yield strength increases with strain rate as observed. Second, we observe that at strain rates 8400 s^{-1} and above, we have an increasing amount of thermal softening.

However, there are two aspects that we do not capture. Recall that we neglect the elastic strain in the model and therefore, we do not capture the initial rise. Similarly, we do not capture the initial stress rise and the subsequent stress oscillations which are well-known artifacts of a split Hopkinson pressure bar.

We elaborate on the results in Fig. 14. We plot the stress, the temperature, the volume fraction of the

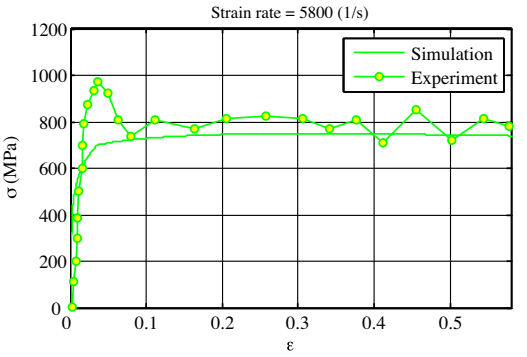

Fig. 9. Stress–strain response of pure iron for a dynamic test, $\dot{\varepsilon} = 5800(\frac{1}{s})$.

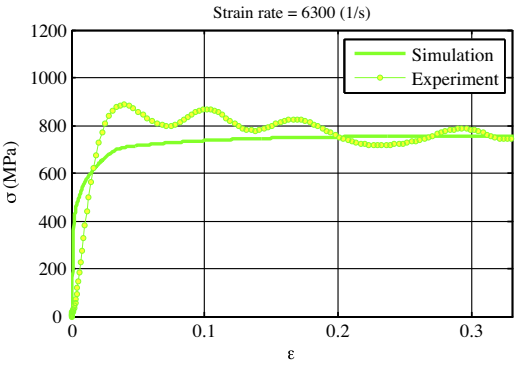

Fig. 10. Stress–strain response of pure iron for a dynamic test, $\dot{\varepsilon} = 6300(\frac{1}{s})$.

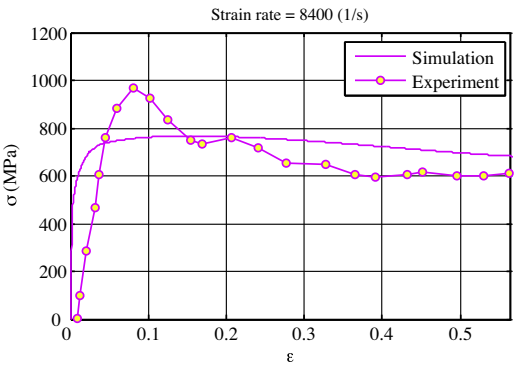

Fig. 11. Stress–strain response of pure iron for a dynamic test, $\dot{\varepsilon} = 8400(\frac{1}{s})$.

martensite and the apparent Taylor–Quinney factor as a function of strain for five different strain rates. Since the strain rates are constant in each test, we may regard the horizontal axes as the (suitably scaled) time. We see that there is virtually no temperature increase in the material for the quasistatic test. This is qualitatively consistent with the observed phenomena in experiments that suggest at low strain rates material has enough time to diffuse the generated heat into the surroundings. At higher strain rates, however, the material does not have enough time

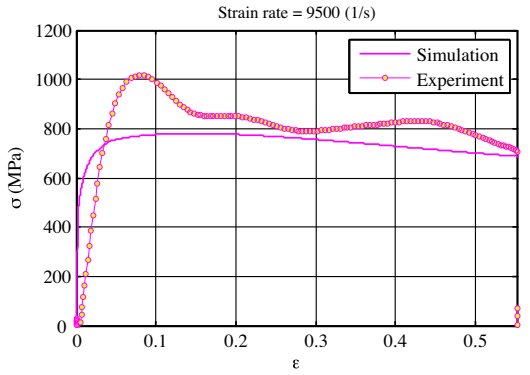

Fig. 12. Stress–strain response of pure iron for a dynamic test, $\dot{\varepsilon} = 9500(\frac{1}{s})$.

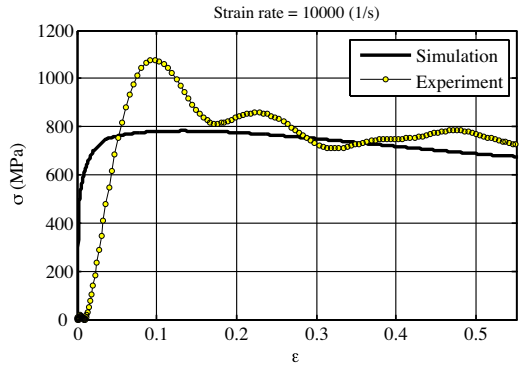

Fig. 13. Stress–strain response of pure iron for a dynamic test, $\dot{\varepsilon} = 10,000(\frac{1}{s})$.

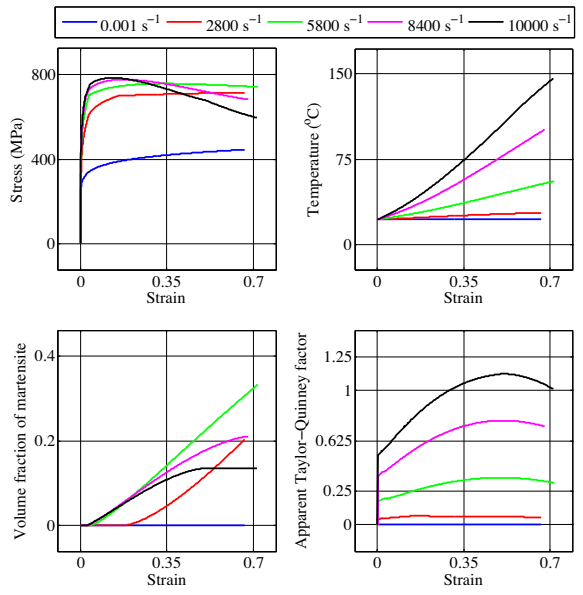

Fig. 14. Theoretical calculation of the progression of phase transformation, stress, temperature and apparent Taylor–Quinney factor for different strain rate experiments.

to conduct out the generated heat and thus temperature of the body increases as deformation proceeds. Further, we also see that the amount of phase transformation increases at intermediate rates and the resulting latent adds to the increasing temperature. All of this is captured by the model. The increasing temperature gives rise to thermal softening at higher strain rates. Further, the increasing temperature and thermal softening at the higher strain rates results in an arrest in the phase transformation finally, we note that it can indeed exceed unity at the highest rate consistent with the observations.

4. Conclusion

In this paper, we have presented a new model that combines martensitic phase transformations with plasticity, and applied it to study the experiments of Rittel et al. (2006) on pure iron. The model builds on the formulation of rate-dependent thermoplasticity proposed by Rosakis et al. (2000) and that of martensitic phase transformations by Sadjadpour and Bhattacharya (2007). We introduce internal variables to describe the phase transformation and plasticity, place them on a consistent thermodynamic framework and prescribe appropriate evolution laws – stick slip model for the phase transformation and Johnson–Cook model for the plasticity. We then specialize the model to a homogenous, adiabatic, constant-strain rate setting as is appropriate for the high-strain rate experiments. We have shown that the model is capable of describing the entire range of experimental observations.

The first significance of the work presented here is that it provides additional support for the presence of $\alpha \Longleftrightarrow \varepsilon$ phase transformation under shear. The experiments of Rittel et al. (2006) provided indirect evidence based on thermal measurements and microstructural characterization that the phase transformation can occur at extremely low levels of stress (of the order of a GPa) in comparison to transformation stress of 13 GPa under shock loading conditions of uniaxial strain (Barker and Hollenbach, 1974) and laser shock experiments (Kalantar et al., 2005). This suggests that the presence of shear can lower the transformation stress significantly, which is consistent with the suggestion made in recent multiscale model proposed for pure iron (Caspersen et al., 2004; Lew et al., 2006). The fact that the current model can describe the rich observations of these experiments supports the presence of phase transitions in these experiments, even though it is not conclusive. Further work with the shear compression specimen (SCS) at high strain rates with in situ diffraction is needed to conclusively assert that the phase transformation is indeed possible in iron at low pressures.

The second significance of the work presented here is that it presents a consistent thermodynamic framework for combining phase transformations and plasticity at high strain-rates. The model could be improved in various ways. First, the model contains no explicit energetic coupling between the phase transformation and plasticity. This is well-known that martensitic $\gamma \Longleftrightarrow \alpha$ transformations promote plasticity. Further, Richards et al. (2013) recently showed that intergranular coupling also promotes a direct

coupling. This could be included by replacing W_p in (7) with a term like $W_h(\zeta, \lambda, \varepsilon_m)$. However, this makes various expressions more complicated and parameter fitting more difficult. Second, the model is macroscopic and contains no microstructural or texture information. As the strain becomes large, the texture can evolve and the constitutive functions can change. Finally, the stored energy of plastic work is specified by the Taylor–Quinney factor β limited to an adiabatic, constant strain-rate setting. Unfortunately we do not have enough independent experimental information at isothermal or other stress states at this time. An important aspect of the combined phase transformation and plasticity in pure iron is the hysteresis observed during loading–unloading in shock wave experiments (Barker and Hollenbach, 1974). A future direction of this modeling would be to explore the behavior of pure iron under shock loading and the observed hysteresis.

Acknowledgments

The work draws from the doctoral thesis of Amir Sadjadpour at the California Institute of Technology. The authors gratefully acknowledge the financial support of the U.S. Department of Energy (GR: Grant No. DE-NA0001805) U.S. Army Research Laboratory (GR & KB: Cooperative Agreement Number W911NF-12-2-0022).

References

Ahrens, T.J., Holland, K.G., Chen, G.Q., 2002. Phase diagram of iron, revised-core temperatures. Geophys. Res. Lett. 29 (Art. no. 1150).
Bancroft, D., Peterson, E.L., Minshall, S., 1956. Polymorphism of iron at high pressure. J. Appl. Phys. 27 (3), 291–299.
Barker, L.M., Hollenbach, R.E., 1974. Shock-wave study of alpha reversible epsilon phase transition in iron. J. Appl. Phys. 45 (11), 4872–4881.
Barton, N.R., Benson, D.J., Becker, R., 2005. Crystal level continuum modelling of phase transformations: the $\alpha \leftrightarrow \epsilon$ transformation in iron. Mod. Sim. Mater. Sci. Eng. 13 (5), 707–731.
Caspersen, K.J., Lew, A., Ortiz, M., Carter, E.A., 2004. Importance of shear in the bcc-to-hcp transformation in iron. Phys. Rev. Lett. 93 (115501).
Chen, G., Ahrens, T.J., 1996. High pressure melting of iron-new experiments and calculations. Philos. Trans. R. Soc. Lond. A354, 1251–1263.
Cherkaoui, M., Berveiller, M., Lemoine, X., 2000. Couplings between plasticity and martensitic phase transformation: overall behavior of polycrystalline TRIP steels. Int. J. Plast. 16 (10–11), 1215–1241.
Clifton, R.J., Klopp, R.W., 1985, . Pressure-Shear Plate Impact Testing, ninth ed., vol. 8. ASM, Metals park, OH, pp. 230–239.
Coleman, R.D., Noll, W., 1963. The thermodynamics of elastic materials with heat conduction and viscosity. Arch. Rat. Mech. Anal. 13 (3), 167–178.
Farren, W.S., Taylor, G.I., 1925. The heat developed during plastic extension of metals. Proc. R. Soc. London A107, 422–451.
Fischer, F.D., Reisner, G., Werner, E., Tanaka, K., Cailletaud, G., Antretter, T., 2000. A new view on transformation induced plasticity (TRIP). Int. J. Plast. 16 (7–8), 723–748.
Follansbee, P.S., 1989. Analysis of the strain-rate sensitivity at high strain rates in fcc and bcc metals. Inst. Phys. Conf. Ser. 102, 213–220.
Jia, D., Ramesh, K.T., Ma, E., 2000. Failure mode and dynamic behavior of nanophase iron in compression. Scr. Mater. 42, 73–78.
Johnson, G.R., Cook, W.H., 1985. Fracture characteristics of three metals subjected to various strains, strain rates, temperatures and pressures. Eng. Fract. Mech. 21, 31–48.
Jones, O.E., Graham, R.A., 1968. Accurate Characterization of the High Pressure Environment, vol. 326. NBS Special Publication, Gaithersburg, MD.
Kalantar, D.H., Belak, J.F., Collins, G.W., Colvin, J.D., Davies, H.M., Eggert, J.H., Germann, T.C., Hawreliak, J., Holian, B.L., Kadau, K., Lomdahl, P.S., Lorenzana, H.E., Meyers, M.A., Rosolankova, K., Schneider, M.S., Sheppard, J., Stolken, J.S., Wark, J.S., 2005. Direct observation of the alpha–epsilon transition in shock-compressed iron via nanosecond X-ray diffraction. Phys. Rev. Lett. 95 (7), 075502.
Klepaczko, J.R., 1969. The strain rate behaviour of iron in pure shear. Int. J. Solids Struct. 5, 533–548.
Leblond, J.B., 1989. Mathematical modelling of transformation plasticity in steels. II: Coupling with strain hardening phenomena. J. Mech. Phys. Solids 5 (6), 573–591.
Leblond, J.B., Devaux, J., Devaux, J.C., 1989. Mathematical modelling of transformation plasticity in steels. I: Case of ideal-plastic phases. J. Mech. Phys. Solids 5 (6), 551–572.
Levitas, V.I., Idesman, A.V., Stein, E., 1998. Finite element simulation of martensitic phase transitions in elastoplastic materials. Int. J. Solids Struct. 35 (9–10), 855–887.
Lew, A., Caspersen, K., Carter, E.A., Ortiz, M., 2006. Quantum mechanics based multiscale modeling of stress-induced phase transformations in iron. J. Mech. Phys. Solids 54 (6), 1276–1303.
Mason, C., Worswick, M.J., 2001. Adiabatic shear in annealed and shock-hardened iron and in quenched and tempered 4340 steel. Int. J. Fract. 111, 29–51.
Millett, J.C.F., Bourne, N.K., Rosenberg, Z., 1997. Shear stress measurements in copper, iron, and mild steel under shock loading conditions. J. Appl. Phys. 81 (6), 2579–2583.
Murr, L.E., Esquivel, E.V., 2004. Observations of common microstructural issues associated with dynamic deformation phenomena: twins, microbands, grain size effects, shear bands, and dynamic recrystallization. J. Mater. Sci. 39 (4), 1153–1168.
Nicolazo, C., Leroy, M., 2002. Dynamic behaviour of α-iron under decremental step pulses. Mech. Mat. 34, 231–241.
Ostwaldt, D., Klepaczko, J.R., Klimanek, 1997. Compression tests of polycrystalline alpha-iron up to high strains over a large range of strain rates. J. Phys. IV France Colloq. C3 7, 385–390.
Richards, A.W., Lebensohn, R.A., Bhattacharya, K., 2013. Interplay of martensitic phase transformation and plastic slip in polycrystals. Acta Mater. 61, 4384–4397.
Rittel, D., Lee, S., Ravichandran, G., 2002. A shear-compression specimen for large strain testing – Springer. Exp. Mech..
Rittel, D., Ravichandran, G., Venkert, A., 2006. The mechanical response of pure iron at high strain rates under dominant shear. Mater. Sci. Eng. A A432, 191–201.
Rosakis, P., Rosakis, A.J., Ravichandran, G., Hodowany, J., 2000. A thermodynamic internal variable model for the partition of plastic work into heat and stored energy in metals. J. Mech. Phys. Solids 48, 581–607.
Rosenberg, Z., Partom, Y., Yaziv, D., 1980. Determination of the dynamic alpha reversible epsilon transformation in iron using manganin stress gauges. J. Phys. D: Appl. Phys. 13 (8), 1489–1496.
Sadjadpour, A., Bhattacharya, K., 2007. A micromechanics inspired constitutive model for shape-memory alloys: the one-dimensional case. Smart Mater. Struct. 16, S51–S62.
Sano, T., Mori, H., Ohmura, E., Myamoto, I., 2003. Femtosecond laser quenching of the epsilon phase of iron. Appl. Phys. Lett. 83 (17), 3498–3500.
Shanthraj, P., Zikry, M.A., 2013. Microstructurally induced fracture nucleation and propagation in martensitic steels. J. Mech. Phys. Solids 61 (4), 1091–1105.
Taylor, G.I., Quinney, H., 1934. The latent energy remaining in a metal after cold working. Proc. R. Soc. London 143, 307–326.
Turteltaub, S., Suiker, A.S.J., 2005. Transformation-induced plasticity in ferrous alloys. J. Mech. Phys. Solids 53 (8), 1747–1788.
Von Barge, N., Boehler, R., 1990. Effect of non-hydrostaticity on the α–ϵ transition of iron. High Pressure Res. 6 (2), 133–140.
Vural, M., Rittel, D., Ravichandran, G., 2003. Large strain mechanical behavior of 1018 cold-rolled steel over a wide range of strain rates. Metal. Mater. Trans. A 34A, 2873–2885.
Watson Jr., H., 1970. Longitudinal wave propagation tests and the experimental determination of the dynamic stress strain characteristics of pure iron. Int. J. Solids Struct. 6 (8), 1157–1172.
Weston, J.M., 1992. Flow stress of shock-hardened remco iron over strain rates from 0.001 to 9000 s^{-1}. J. Mater. Sci. Lett. 11, 1361–1363.
Yaakobi, B., Boehly, T.R., Meyerhofer, D.D., Collins, T.J.B., Remington, B.A., Allen, P.G., Pollaine, S.M., Lorenzana, H.E., Eggert, J.H., 2005. Exafs measurement of iron bcc-to-hcp phase transformation in nanosecond-laser shocks. Phys. Rev. Lett. 95 (7), 075501.